

Carbon-Supported Palladium Sub-Nanometer Particle Catalyst for Oxygen Reduction Reaction in Acid Media

Jun Ho Shim, Hyun Jung Jung, Youngmi Lee,* and Chongmok Lee*

Department of Chemistry and Nano Science, Ewha Womans University, Seoul 120-750, Korea

Received July 6, 2011; E-mail: cmlee@ewha.ac.kr, youngmilee@ewha.ac.kr

Pd nanoparticles (Pd NPs) on a carbon support (Pd/C) were synthesized in ethylene glycol containing poly(1-vinyl-2-pyrrolidone) (PVP) at various PVP/Pd precursor ratios. The sizes of the Pd NPs were controlled by varying the PVP concentration. Smaller Pd NPs were obtained at higher PVP concentrations. Indeed, the mean sizes of the Pd NPs with PVP/Pd precursor ratios of 0, 40, and 80 (Pd/C-0, -40, and -80) were 2.8 (±1.2), 1.5 (±0.3), and 0.8 (±0.3) nm, respectively, by TEM analysis. The electrocatalytic activities of the Pd/C catalysts toward the oxygen reduction reaction (ORR) were examined in a 0.1 M $HClO_4$ solution using rotating disk electrode voltammetry. The smaller Pd NPs exhibited more efficient ORR properties, such as a more positive ORR onset potential (or half-wave potential, $E_{1/2}$) and increased number of electrons (n) transferred in the ORR. In particular, the Pd/C-80 catalyst with a lower metal content (7.9 wt % Pd) showed desirable ORR performance in terms of the onset potential, n value, mass activity, and methanol tolerance.

The electrocatalytic activity of metals for the oxygen reduction reaction (ORR) is of great interest, particularly in the field of fuel cells. Carbon-supported Pt nanoparticle (NP) catalysts are used most commonly as cathode catalysts because they show high activity toward a sluggish ORR.[1,2] In general, the size of the Pt NPs is also an important factor for electrocatalytic reactions in fuel cells.[3–5] However, the high cost and limited supply of Pt as well as the requirement of a high Pt loading have impeded the wide spread applications of ORR. In addition, Pt-based anodes are readily poisoned by carbon monoxide during fuel oxidation, which is another drawback of Pt.[1,6] For these reasons, a great deal of research has focused on the development of electrode materials as a replacement for Pt. In this respect, Pd NPs have attracted attention as substitutes for Pt NPs considering Pt and Pd belong to the same group in the periodic table and have similar properties. However, a large number of reports regarding fuel cell anodes and cathodes have used Pd–M alloy NPs rather than pure Pd NPs[1,2] because the ORR activity of Pd alone is still lower than that of Pt.[7]

The preparation of Pd NPs with controlled particle sizes has attracted considerable research attention. For example, the preparation techniques employed for Pd NPs included thermal treatment,[8] chemical[9–13] or electrochemical[14,15] reduction of metal precursors in the presence of a stabilizer, such as linear polymers,[9] poly(1-vinyl-2-pyrrolidone) (PVP),[16,17] ligands,[10] ionic liquid,[11] alkanethiol,[12] and surfactants,[13] which prevent the NPs from aggregating. However, it is difficult to find reports dealing with the size effect of pure Pd NPs on the ORR activity. Recently, Jiang et al. reported the size dependence of Pd particles on the ORR activity in alkaline media,[8] where the size of Pd NPs was controlled by the heat treatment of a commercial 20 wt % Pd/C catalyst at temperature ranging from 300 to 600 °C.

In general, the particle size of metal catalysts is related to the active surface area, which in turn affects the catalytic activity. To the best of the authors' knowledge, there are no reports on the Pd NP size dependence of the ORR activity in acid media, which might be due to the unstable properties and relatively lower catalytic activity compared to Pt NPs.[7] Only a few studies have investigated the ORR activity in acid media with a specific size of Pd NP.[18–20] This paper reports the synthesis of size-controlled Pd NPs (a few to sub-nanometers in diameter) by varying the concentration of protecting agent PVP, and the size-dependent ORR catalytic activity of the prepared Pd NPs. These results are of importance for the development of Pd NP catalysts in ORR including their size effect. For comparison, the same measurements were made with an E-TEK commercial Pt catalyst.

Experimental

Reagents and Instruments. All solvents and chemicals were of analytical-reagent grade and all solutions were prepared using 18 MΩ cm^{-1} deionized water. Commercial carbon-supported Pt catalyst (20 wt % Pt loading on Vulcan XC-72) was purchased from E-TEK Co. and denoted as Pt/C. Analytical-reagent grade ethylene glycol (EG) was obtained from Acros, Pd precursor salts, i.e., $PdCl_2$, and carbon black (acetylene) were purchased from Alfa Aesar. PVP (MW: 55000, a stabilizer for Pd NPs), and Nafion (5.0 wt % solution) was obtained from Aldrich. All chemicals were used as received. The shape and size of the as-synthesized Pd NPs were characterized by transmission electron microscopy (TEM, JEM 2100F) operating at an accelerating voltage of 200 kV. The phase structures were examined by X-ray diffraction (XRD; Siemens D500, with a Cu Kα radiation). The Pd NPs content was determined by inductively coupled plasma atomic emission spectroscopy (ICP-AES) with an OPTIMA 4300 DV (Perkin-Elmer).

Published on the web November 9, 2011; doi:10.1246/bcsj.20110206

Synthesis of Pd NPs. In a typical synthesis, 20 mL of 1.0 mM $PdCl_2$ with various concentrations of PVP (0, 40, and 80 mM) in EG was stirred in a 100 mL three-necked round bottom flask. The resulting mixture was then sonicated for 30 min to promote the dissolution of PVP.[16] The concentration of PVP was calculated as a monomeric unit. To promote the dispersion of Pd metal NPs, a supporting carbon material (2 mg mL^{-1}) was added to the flask and the flask was capped. Subsequently, the pH of the reaction mixture was adjusted to 11 by adding 1.0 M NaOH dropwise. The reaction solution was then heated under reflux at 160 °C for 10 min, followed by cooling to room temperature. The final product, carbon supported Pd NPs (Pd/C), was obtained by centrifugation, and washed with acetone once and then twice with ethanol to remove the unreacted EG. The product was finally dried overnight under vacuum.

Electrochemical Measurements. Prior to electrode surface modification, the glassy carbon (GC) rotating disk working electrode (RDE; 0.071 cm^2) was wet-polished on an Alpha A polishing cloth (Mark V Lab) using 0.3 and 0.05 μm aluminum slurries, successively. The electrode was then rinsed with distilled water, and finally sonicated in distilled water for 60 s to remove the residual aluminum slurry from the electrode surface. The catalyst-loaded GC electrode was prepared by casting a 5.0 μL aliquot of each Pd/C suspension (1 mg mL^{-1}), twice for 5 min each, and allowed to dry for 2 h. After evaporating the water at room temperature, the modified electrode was coated with 10.0 μL of a 0.05 wt% Nafion solution to capture the catalyst on the electrode surface. The electrode was finally dried at room temperature for 2 h. A large-area Pt coil served as the counter electrode, and a saturated calomel electrode (SCE) was used as the reference electrode. The RDE measurements and cyclic voltammetry (CV) were performed using a RDE-1 of BAS (Bioanalytical System) and an electrochemical analyzer (CH Instrument, 705D), respectively. The measured currents were converted to the current density by normalization to the geometric surface area (GSA) of each modified electrode, which was determined by chronocoulometry (CC) in a 10 mM $K_3[Fe(CN)_6]$ aqueous solution containing 0.1 M KCl as the supporting electrolyte. The ORR was studied in an O_2 saturated 0.1 M $HClO_4$ solution.[21] The solution was purged with O_2 for 30 min before each measurement and a flow of O_2 gas was maintained over the solution surface during the experiment to maintain a constant concentration. The ORR currents were recorded at electrode rotating speeds from 100 to 3600 rpm (scan rate = 5 mV s^{-1}, potential range = −0.05 and 0.65 V vs. SCE).

Results and Discussion

Characterizations of Size-Controlled Pd NPs. To examine the size effect of Pd NPs, the aim was to obtain the smallest particles possible. It was reported that the particle size decreases with increasing boiling point of the alcohol and the PVP/Pd precursor ratios.[16] To obtain small NPs, EG was chosen as a reducing agent because its high boiling point and PVP/Pd precursor ratios (0, 40, and 80) were varied. The other synthetic conditions were referenced from the literature.[22] Briefly, EG was used as both a solvent and as a reducing agent for the reduction of metal ions and PVP as a stabilizing agent in the presence of supporting carbon material at pH 11. The resulting carbon supported Pd NPs (Pd/C) as Pd/C-0, -40, and -80 depending on PVP/Pd precursor ratios, respectively.

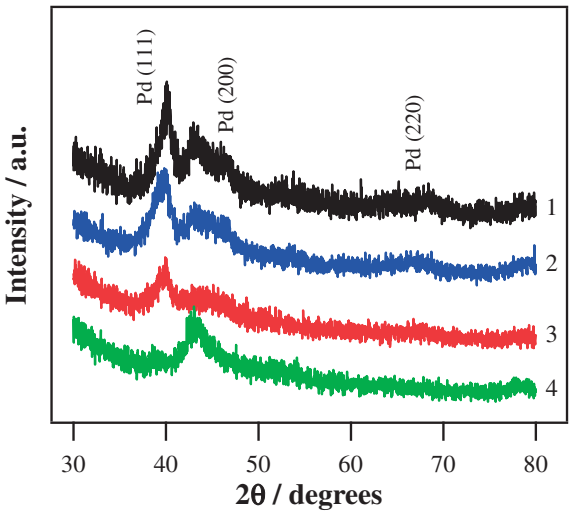

Figure 1. XRD patterns of (1) Pd/C-0, (2) Pd/C-40, (3) Pd/C-80, and (4) carbon.

Figure 1 shows XRD patterns of the series of Pd/C catalysts. The peaks at approximately 40.1 could be attributed to the crystal facet of the Pd(111) diffraction peak. The other peaks at approximately 46.5 and 68.4, attributed to Pd(200) and Pd(220), did not show good enough S/N ratio for applying the Scherrer equation presumably due to both the small Pd size and the presence of carbon.[23] Despite this point, if we apply the Scherrer equation the particle sizes of Pd/Cs are 4–6 nm. Therefore, the mean Pd particle sizes in the Pd/C catalysts were also estimated from the TEM images. Note that a shift in the diffraction angle of Pd(111) toward a lower value in Pd/C-40 and -80 was observed, indicating an expansion of the Pd–Pd interatomic distance.[16]

Figure 2 shows typical TEM images and the corresponding size distributions of the Pd NPs prepared in the presence of different concentrations of PVP. The individual NPs were well-dispersed and the Pd NP sizes were controlled by varying the amount of PVP, whereas the particle sizes became larger and were not readily controlled in the absence of PVP. From the histograms for the particle size distributions obtained from the TEM images, the mean diameters of the Pd NPs in Pd/C-0, -40, and -80 were 2.8 (±1.2), 1.5 (±0.3), and 0.8 (±0.3) nm, respectively, where 50 particles were quantified for each case by magnifying TEM images at various places. This shows that the particle size can be controlled by the PVP concentration. On the other hand, PVP concentrations >80 mM could not be achieved due to the difficulty in dispersing PVP in EG. Table 1 lists the particle size and metal content of the catalysts.

Figure 3 shows the Pd/C catalysts characterized by CV. In the presence of Pd NPs, each CV has three distinctive regions, a double layer region, a hydrogen region, and an oxide region. For the Pd/C-modified GC electrodes, a large increase in the background current was observed in the presence of the supporting carbon material. Indeed, rather small peaks corresponding to hydrogen absorption–desorption were observed in the case of Pd/C-0, indicating that the larger particle size of

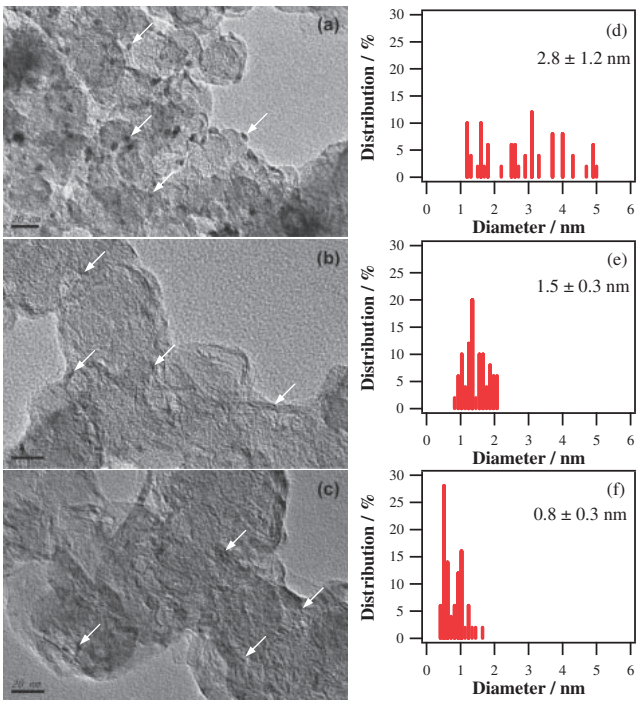

Figure 2. TEM images and size distribution histograms of the Pd/C catalysts synthesized with (a and d) 0, (b and e) 40, and (c and f) 80 mM of PVP. A few representative particles are marked by arrows. The scale bars are 20 nm.

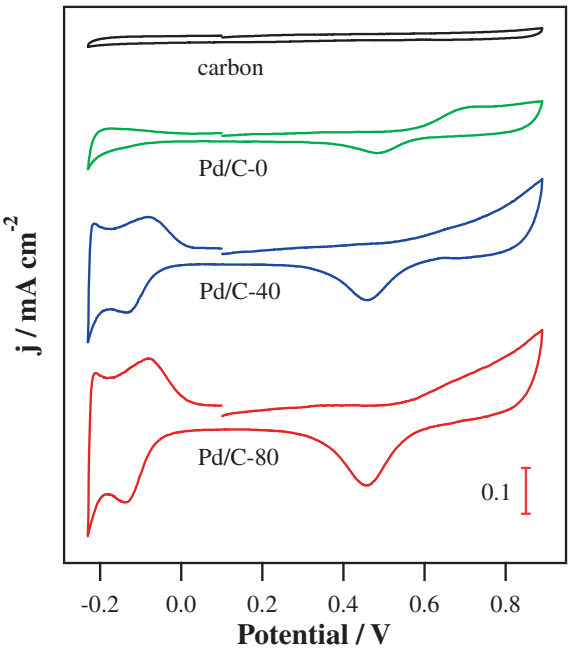

Figure 3. Representative CVs obtained at Pd/C-modified electrodes in an Ar-saturated 0.1 M $HClO_4$ solution at a scan rate of 10 mV s^{-1}.

Table 1. Structural and Electrochemical Characteristics of the Pt/C and Pd/C Electrocatalysts

Electrode	Particle size[a] /nm	ICP-AES /wt %	GSA[b] /cm^2	Exposed metal surface area[c] /cm^2	Onset potential /V	$E_{1/2}$ /V	n[d]
Pt/C	2.5	22.4	0.080	1.411	0.605	0.472	3.84
Pd/C-0	2.8 ± 1.2	6.3	0.097	0.160	0.570	0.236	—
Pd/C-40	1.5 ± 0.3	10.7	0.107	0.340	0.570	0.415	3.73
Pd/C-80	0.8 ± 0.3	7.9	0.112	0.640	0.615	0.464	4.04

a) Estimated from TEM images except commercial Pt/C that is taken from reference.[24] b) Calculated from the slope of Q vs. $t^{1/2}$ obtained from the plots of chronocoulograms. c) Surface area of exposed metal calculated using the charges corresponding to hydrogen adsorption and desorption with conversion factor of 210 μC cm^{-2} for Pt/C; and monolayer Pd oxide reduction with a conversion factor of 310 μC cm^{-2} for Pd/C.[25,26] d) Calculated from the current densities recorded at a potential of 0.0 V vs. SCE.

Pd/C-0 decreased the net exposed active Pd surface area of the electrocatalyst. The cathodic peak currents of the Pd/C catalysts with smaller Pd particle sizes (Pd/C-40 and Pd/C-80) at 0.46 V corresponding to the Pd oxide reduction were relatively larger than those with larger Pd particle sizes (Pd/C-0). Note that these CVs alone imply not only high exposed Pd surface area of Pd/C-40 and -80 but also small particle sizes due to well-defined hydrogen adsorption–desorption peaks, characteristics of the reduced size of Pd.[18] Although TEM images might mislead one to believe the particles are smaller than the real sizes, we believe, the real particle sizes are smaller than those obtained from the Scherrer equation by the following rational: (1) well-defined adsorption/desorption of hydrogen peaks in CV; (2) shift in the diffraction angle of Pd(111) toward a lower value in Pd/Cs; (3) averaging 50 particles of TEM images.

ORR at the Catalysts. The catalytic performance of bulk Pt (bPt), Pt/C, Pd/C-0, Pd/C-40, and Pd/C-80 toward the ORR was examined by RDE voltammetry, where Pt disk RDE served as bPt. The results are presented as the current densities vs. potential. The current densities were obtained by normalizing the measured currents to the corresponding electrode GSA. The GSAs were estimated from the slopes obtained by CC experiments according to the integrated Cottrell equation as reported previously.[27] The GSAs were greater (ca. 0.097–0.112 cm^2 depending on the catalyst loadings) than that of the substrate GC electrode (0.071 cm^2). This suggests that the Pd/C catalysts appear to be loaded even over the insulator of the GC electrode, resulting in an enlarged GSA.

RDE voltammetry was performed with the electrode loaded with each catalyst at a range of electrode rotating speeds in 0.1 M $HClO_4$ saturated with O_2.[21] Figure 4 shows the RDE

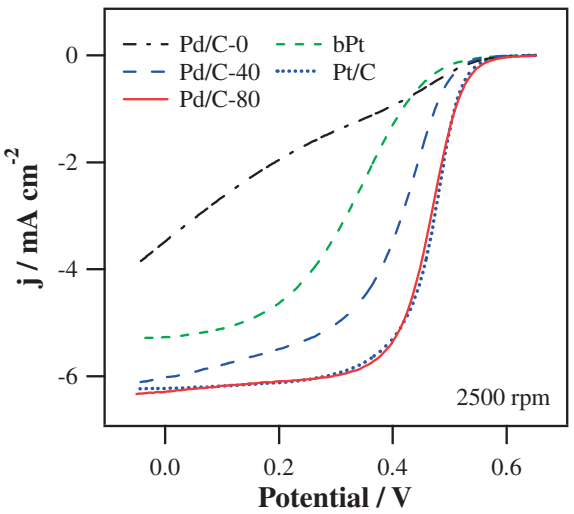

Figure 4. RDE voltammetry curves of bPt, Pt/C, Pd/C-0, Pd/C-40, and Pd/C-80 in 0.1 M $HClO_4$ saturated with O_2 at 2500 rpm (scan rate, 5 mV s^{-1}).

voltammetry curves acquired at 2500 rpm. The ORR on the Pd/C-0 catalyst is under mixed kinetic and diffusion control in the potential window between 0.65 and −0.05 V. The addition of PVP increases the ORR activity of Pd NPs significantly as observed with Pd/C-40 and Pd/C-80 compared to Pd/C-0. The improvement in activity with decreasing Pd NP size appears to be due mainly to two factors. The first is an enlargement of the electroactive surface area of Pd. Although reduction of the surface oxide is not a direct measure of the ORR activity, the observed ORR activity of the catalysts also corresponded to the order of the surface oxide reduction peak area, which might be considered as the electroactive Pd surface area, (Pd/C-80 > Pd/C-40 > Pd/C-0), as summarized in Table 1. This tendency concurs with previous results in gold activation.[27] The other factor in the ORR activity is believed to be a dilation of the Pd–Pd interatomic distance as the size of the Pd NP decreases,[16] which might provide a similar interatomic distance to Pt–Pt. Note that the value of the lattice parameter of pure Pt metal is slightly larger than that of pure Pd metal, 0.3923 and 0.3890 nm, respectively.[1] In the case of Pd/C-40 and Pd/C-80, the onset potential for ORR, which is defined as the potential at which the current begins to fall below zero, was found to be 0.570 and 0.615 V, respectively (Table 1). We estimated the onset potential where the cathodic current exceeds four times the standard deviation of the S/N ratio. For the comparison of the catalytic activities, we also presented half-wave potential ($E_{1/2}$) values which are often used as criteria for the catalytic activity (Table 1).[21] Indeed, increasing the PVP content contributed further to the improvement of the catalyst activity. The Pd/C-80 and Pt/C catalysts exhibit a similar limited current density. Regarding the RDE voltammetric curve shape, a sharper slope in the RDE curve was observed for Pd/C-80 and Pt/C, indicating that the Pd/C-80 catalyst shows faster ORR kinetics. Considering the ORR onset potential, the overall catalytic activity for the ORR on the catalysts increases in the order of bPt < Pd/C-0 ≈ Pd/C-40 < Pt/C ≈ Pd/C-80. In terms of half-wave potential, the order is Pd/C-0 < bPt < Pd/C-40 < Pd/C-80 ≈ Pt/C. This suggests that a reduced particle size concomitant with a change in the interatomic distance, Pd/C-80, may facilitate oxygen adsorption on the catalyst surface, resulting in enhanced ORR kinetics. Note, however, the reported $E_{1/2}$ value for Pt/C is 0.82–0.89 V vs. RHE depending on the electrolyte condition and state of catalyst, which is better than that of the present study (0.71 V vs. RHE).[21] This discrepancy comes from impurities in the electrolyte solution and/or the matter of state-of-the-art of electrode fabrication.

ORR Kinetics and Methanol Tolerance at the Catalysts. The number of electrons (n) transferred during the course of ORR at each electrode can be evaluated by considering the Koutechy–Levich (K–L) equation:[28]

$$\frac{1}{j} = \frac{1}{j_k} + \frac{1}{j_d} = -\frac{1}{nFkC^0} - \frac{1}{0.62nFD_O^{2/3}v^{-1/6}C^0\omega^{1/2}} \quad (1)$$

where j is the measured current density, j_k and j_d are the kinetic and diffusion-limited current densities, respectively, k is the rate constant for the ORR, F is the Faraday constant, ω is the rotation rate, C^0 (1.18×10^{-6} mol cm^{-3}) is the saturated concentration of oxygen, D_O (1.90×10^{-5} cm^2 s^{-1}) is the diffusion coefficient of oxygen, and v is the kinematic viscosity of the solution (1.1×10^{-2} cm^2 s^{-1}). The parameters for the calculation were obtained from the literature.[29,30] Figure 5a shows the dependence of the RDE curves for the ORR on the rotation rate of the Pd/C-80 loaded electrode. Figure 5b presents the K–L plot for Pd/C-80 based on the RDE data in Figure 5a and that for Pt/C using the RDE data obtained in a similar way. The n values for the other catalysts were also calculated from the slopes of the K–L plots using the RDE current densities at 0.0 V, which were 3.84, 3.73, and 4.04 for the Pt/C, Pd/C-40, and Pd-80 catalysts, respectively (Table 1). The K–L plot was not performed for the Pd/C-0 electrode because eq 1 was developed in the diffusion-limited region, whereas the ORR current for Pd/C-0 was still in the kinetic-controlled region, as shown in Figure 4. The n values for Pt/C and Pd-80 were close to four, indicating that the desirable direct four-electron pathway was dominant. Interestingly, the observed ORR onset potentials and calculated n values decreased simultaneously in the order Pd/C-80 ≥ Pt/C > Pd/C-40, suggesting that the ORR activity of Pd/C-80 is comparable to commercial Pt/C with respect to these two ORR activity parameters. Almost identical slopes in the K–L plots observed at 0.0–0.4 V indicates the ORR at Pd/C-80 is totally mass-transfer controlled in this potential region contrast to our previous results on the activated Au and metal–polythiophene catalysts.[27,31]

For three efficient catalysts, Pt/C, Pd/C-40 and -80, mass-transport-corrected Tafel plots were also constructed in the mixed kinetic-diffusion-controlled regime according to eq 2.

$$E = E^0 - b\log j_k + b\log j_0 \quad (2)$$

where j_o is the exchange current density, b is 2.303 $RT/\alpha nF$ (α: transfer coefficient), and j_k is expressed as the following equation from a rearrangement of eq 1:

$$j_k = \frac{j \times j_d}{j_d - j} \quad (3)$$

The Tafel plots for the catalysts were independent of the rotation speed in the range of 100–3600 rpm. Typical Tafel plots for the RDE voltammetric results obtained at a rotation speed of 2500 rpm were obtained in the potential range from 0.60 to 0.46 V, where Tafel slope at low current density region was used to obtain j_k in the mixed kinetic-diffusion-controlled region by mass-transport-correction (Figure 6). The Tafel slopes of the ORR curves for the Pd/C and Pt/C are close to 0.060 V decade^{-1}.

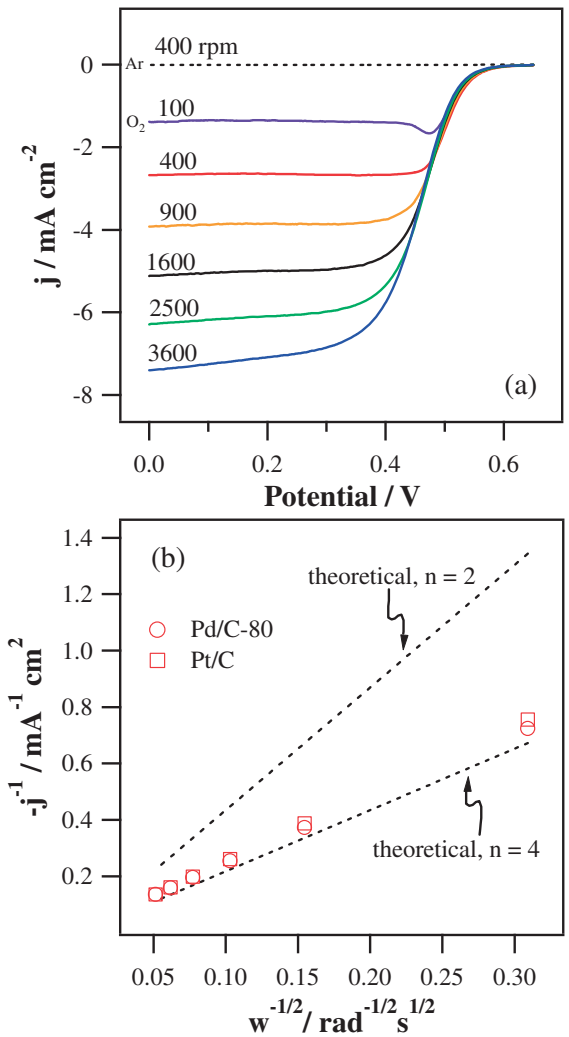

Figure 5. (a) RDE voltammetry curves for the ORR at Pd/C-80 loaded electrode obtained at a range of rotation speeds and (b) corresponding Koteckey–Levich plots for (○) Pd/C-80 and (□) Pt/C at 0.0 V in 0.1 M $HClO_4$ saturated with O_2 (scan rate, 5 mV s^{-1}).

For further analysis of the catalytic activity, the kinetic current densities were normalized to the GSA of the electrodes ($j_{k,GSA}$) and to the mass of Pd or Pt on the electrodes ($j_{k,mass}$), and the catalysts were compared (Table 2). The $j_{k,GSA}$ at 0.55 V for Pd/C-40, Pd/C-80, and Pt/C calculated from Figure 5 was 0.07, 0.24, and 0.18 mA cm^{-2}, respectively. The $j_{k,mass}$ at 0.55 V for Pd/C-40, Pd/C-80, and Pt/C were 3.4, 16.7, and 3.2 mA mg^{-1}, respectively, recalling the wt % of metal in Pd/C-80 is approximately one third of that in Pt/C (Table 1). In addition, remarkable improvement in the ORR activity was observed as the size of the Pd NPs decreased from 1.5 to 0.8 nm: the $j_{k,GSA}$ and $j_{k,mass}$ of Pd/C increased 3.4 and 4.9 fold, respectively. Interestingly, the $j_{k,GSA}$ and $j_{k,mass}$ of Pd/C-80 at 0.55 V was a factor of 1.3 and 5.3 greater than that of Pt/C, respectively.

The j_o values, which are considered to be an indicator for the catalyst ORR activity, were also calculated from an extrapolation of the Tafel plots to $E = E^o$ (standard reduction potential) according to eq 2. E^o for the four-electron transfer ORR was 0.988 V vs. SCE under these experimental conditions. The $j_{o,GSA}$ values of Pd/C-40, Pd/C-80, and Pt/C were similar. On the other hand, the $j_{o,mass}$ value of ORR on Pd/C-80 was four times larger than that of Pt/C, which suggests that more favorable ORR kinetics would be obtained on Pd/C-80 than Pt/C, which is in conformity with the observation of j_k at 0.55 V, n values, and ORR onset potentials.

Stability of Pd/C-80 has also been examined by repetitive RDE experiments in an O_2-saturated 0.1 M $HClO_4$ solution.

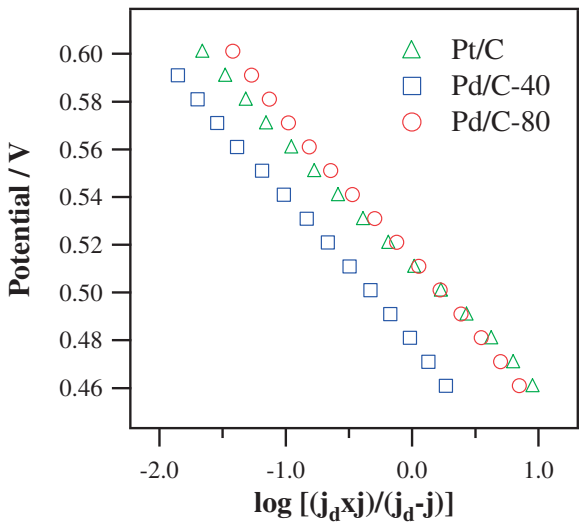

Figure 6. Tafel plots of the ORR obtained for (△) Pt/C, (□) Pd/C-40, and (○) Pd/C-80 from the RDE voltammetry curves (Figure 3) at electrode rotation rate of 2500 rpm.

Table 2. ORR Kinetic Parameters Obtained for the Pt/C and Pd/C Electrocatalysts[a)]

Electrode	$j_{k,GSA}$ /mA cm^{-2}	$j_{k,mass}$ /mA mg^{-1}	j_o /10^{-6} A cm^{-2}	j_o /10^{-4} A mg^{-1}	b /V decade^{-1}
Pt/C	0.177	3.17	8.1	2.9	0.060
Pd/C-40	0.068	3.42	8.0	8.0	0.064
Pd/C-80	0.236	16.71	8.3	11.8	0.057

a) Calculated from the Tafel plots, and j_k values were taken at 0.55 V.

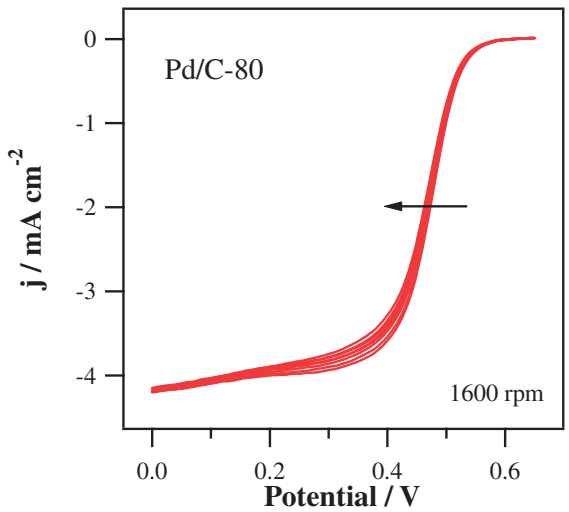

Figure 7. RDE voltammograms for the ORR obtained repetitively for 18 runs in an O_2-saturated 0.1 M $HClO_4$ at Pd/C-80 (rotation speed = 1600 rpm; scan rate = 5 mV s^{-1}). Arrows indicate the order of RDE runs from first to 18th.

Figure 7 shows the RDE voltammetry curves obtained during 18 repetitive runs. They exhibited negative shift of the RDE curves but maintained limiting current densities at 0.0 V as the number of RDE runs increased. Of course, stability of Pd/C-80 is not as good as Pt base catalyst. However, we think, the stability of Pd/C-80 under acidic solution is not that bad for a Pd-based catalyst. Rather, this result may suggest some possibility of using Pd cathode under acidic solution by proper improving treatment, say, Au-modification.[32]

One of the drawbacks of Pt-based catalyst cathodes regarding direct methanol fuel cells (DMFCs) is the problem of methanol crossover through the polymer electrolyte.[1] Platinum is known to have the highest catalytic activity for oxygen reduction among pure metals but provides strong adsorptive sites for methanol, which results from ORR and methanol oxidation occurring simultaneously at the mixed potential in air electrode. In our CV experiments in the presence and absence of methanol, Pd/C-80 showed very low activity for methanol oxidation in contrast to Pt/C (Figure 8). In fact, the peak (≈0.4 V) observed at Pt/C in the reverse scan corresponds to the oxidation of adsorbed species produced from methanol oxidation and this carbon species adsorption is the main reason for the catalyst activity decrease. In contrast, Pd/C-80 did not show the peak corresponding to the adsorbed species due to its lower methanol oxidation activity. Nevertheless the Pd/C-80 exhibited high activity for oxygen reduction comparable to Pt/C (Figure 4). In other words, Pd-80 has high ORR activity but low methanol oxidation activity within our experimental conditions and therefore it could be a good cathode catalyst in fuel cells.

Conclusion

A few to sub-nanometer-sized Pd particles supported on carbon (Pd/C) were synthesized by EG and PVP. The RDE experiments with the Pd/C-modified electrode in the acidic media confirmed the efficient four-electron transfer ORR. The

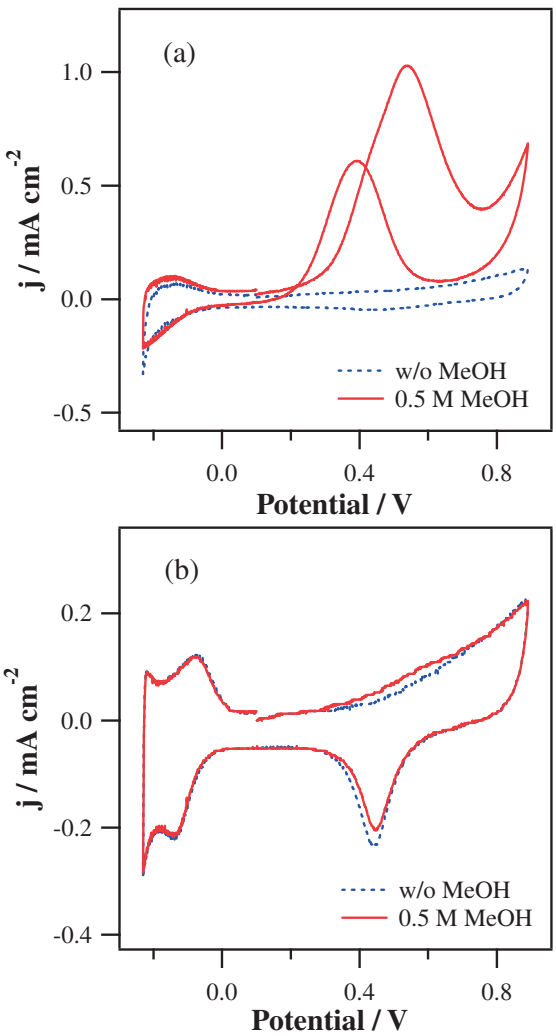

Figure 8. Cyclic voltammograms at (a) Pt/C, and (b) Pd/C-80 catalysts recorded in 0.1 M $HClO_4$ solution in presence (solid line) and absence (dotted line) of 0.5 M CH_3OH saturated with Ar (scan rate, 10 mV s^{-1}).

ORR activity of Pd/C was dependent on the particle size. Indeed, the ORR activity was improved as the size of the Pd NPs decreased from 1.5 to 0.8 nm, i.e., both the $j_{k,GSA}$ and $j_{k,mass}$ of Pd/C increased by 3.4 and 4.9 times, respectively. In particular, the Pd/C-80-modified electrode showed desirable performance from the viewpoint of the onset potential, normalized kinetic activity, and methanol tolerance. The observed better ORR activity of the smaller Pd NPs was attributed to the following two factors. One is obviously due to the enlarged surface area per unit volume of the Pd NPs providing more active sites. The other is believed to be an expansion of Pd–Pd interatomic distance with decreasing Pd NP size. Moreover, the Pd wt% in Pd/C-80 was only 35% of the Pt wt% in Pt/C, which is another merit of Pd/C-80, considering the high cost and rarity of these novel metals.

We appreciate the referees' comments for making our presentation much clearer in the course of revision of this paper. This research was carried out under the General R/D Program of the Daegu Gyeongbuk Institute of Science and

Technology (DGIST), funded by the Ministry of Education, Science and Technology (MEST) of the Republic of Korea. J. H. Shim was supported by RP-Grant 2009 of Ewha Womans University.

References

1 E. Antolini, *Energy Environ. Sci.* **2009**, *2*, 915.
2 B. Wang, *J. Power Sources* **2005**, *152*, 1.
3 K. J. J. Mayrhofer, B. B. Blizanac, M. Arenz, V. R. Stamenkovic, P. N. Ross, N. M. Markovic, *J. Phys. Chem. B* **2005**, *109*, 14433.
4 S. Zhang, Y. Shao, G. Yin, Y. Lin, *J. Mater. Chem.* **2009**, *19*, 7995.
5 F. Su, Z. Tian, C. K. Poh, Z. Wang, S. H. Lim, Z. Liu, J. Lin, *Chem. Mater.* **2010**, *22*, 832.
6 V. Mazumder, Y. Lee, S. Sun, *Adv. Funct. Mater.* **2010**, *20*, 1224.
7 O. Savadogo, K. Lee, K. Oishi, S. Mitsushima, N. Kamiya, K.-I. Ota, *Electrochem. Commun.* **2004**, *6*, 105.
8 L. Jiang, A. Hsu, D. Chu, R. Chen, *J. Electrochem. Soc.* **2009**, *156*, B643.
9 Y. Wang, M. Du, J. Xu, P. Yang, Y. Du, *J. Dispersion Sci. Technol.* **2008**, *29*, 891.
10 C. Amiens, D. de Caro, B. Chaudret, J. S. Bradley, R. Mazel, C. Roucau, *J. Am. Chem. Soc.* **1993**, *115*, 11638.
11 J.-H. Cha, K.-S. Kim, H. Lee, *Korean J. Chem. Eng.* **2009**, *26*, 760.
12 S. Chen, K. Huang, J. A. Stearns, *Chem. Mater.* **2000**, *12*, 540.
13 P.-F. Ho, K.-M. Chi, *Nanotechnology* **2004**, *15*, 1059.
14 L. Xiao, L. Zhuang, Y. Liu, J. Lu, H. D. Abruña, *J. Am. Chem. Soc.* **2009**, *131*, 602.
15 W. Pan, X. Zhang, H. Ma, J. Zhang, *J. Phys. Chem. C* **2008**, *112*, 2456.
16 T. Teranishi, M. Miyake, *Chem. Mater.* **1998**, *10*, 594.
17 L.-J. Chen, C.-C. Wan, Y.-Y. Wang, *J. Colloid Interface Sci.* **2006**, *297*, 143.
18 J. J. Salvador-Pascual, S. Citalán-Cigarroa, O. Solorza-Feria, *J. Power Sources* **2007**, *172*, 229.
19 J.-S. Zheng, X.-S. Zhang, P. Li, J. Zhu, X.-G. Zhou, W.-K. Yuan, *Electrochem. Commun.* **2007**, *9*, 895.
20 L. Cheng, Z. Zhang, W. Niu, G. Xu, L. Zhu, *J. Power Sources* **2008**, *182*, 91.
21 Y. Garsany, O. A. Baturina, K. E. Swider-Lyons, S. S. Kocha, *Anal. Chem.* **2010**, *82*, 6321.
22 L. S. Sarma, C.-H. Chen, S. M. S. Kumar, G.-R. Wang, S.-C. Yen, D.-G. Liu, H.-S. Sheu, K.-L. Yu, M.-T. Tang, J.-F. Lee, C. Bock, K.-H. Chen, B.-J. Hwang, *Langmuir* **2007**, *23*, 5802.
23 S. Domínguez-Domínguez, Á. Berenguer-Murcia, B. K. Pradhan, Á. Linares-Solano, D. Cazorla-Amorós, *J. Phys. Chem. C* **2008**, *112*, 3827.
24 R. Hsu, Z. Chen, *ECS Trans.* **2009**, *25*, 1169.
25 S. Trasatti, O. A. Petrii, *Pure Appl. Chem.* **1991**, *63*, 711.
26 M. Hara, U. Linke, Th. Wandlowski, *Electrochim. Acta* **2007**, *52*, 5733.
27 J. H. Shim, J. Kim, C. Lee, Y. Lee, *J. Phys. Chem. C* **2011**, *115*, 305.
28 A. J. Bard, L. R. Faulkner, *Electrochemical Methods: Fundamentals and Applications*, 2nd ed., John Wiley & Sons, New York, **2001**.
29 U. A. Paulus, A. Wokaun, G. G. Scherer, T. J. Schmidt, V. Stamenkovic, V. Radmilovic, N. M. Markovic, P. N. Ross, *J. Phys. Chem. B* **2002**, *106*, 4181.
30 D. Nguyen-Thanh, A. I. Frenkel, J. Wang, S. O'Brien, D. L. Akins, *Appl. Catal., B* **2011**, *105*, 50.
31 S. J. Han, H. J. Jung, J. H. Shim, H.-C. Kim, S.-J. Sung, B. Yoo, D. HaLee, C. Lee, Y. Lee, *J. Electroanal. Chem.* **2011**, *655*, 39.
32 J. Zhang, K. Sasaki, E. Sutter, R. R. Adzic, *Science* **2007**, *315*, 220.